Solar Energy 181 (2019) 372–378

Contents lists available at ScienceDirect

Solar Energy

journal homepage: www.elsevier.com/locate/solener

Electron and hole transport layers optimization by numerical simulation of a perovskite solar cell

Faiza Azri, Afak Meftah, Nouredine Sengouga*, Amjad Meftah

LMSM, Université de Biskra, BP 145RP, 07000 Biskra, Algeria

ARTICLE INFO

Keywords:
Perovskite
Simulation
ETL
HTL
Power conversion efficiency
Defects

ABSTRACT

In this paper an n-i-p perovskite solar cell was studied using SCAPS simulator. The primary solar cell's structure is FTO/ITO/Perovskite/PEDOT:PSS/Au which has achieved a power conversion efficiency of $\eta \sim 13.94\%$. In order to enhance its performance, several materials were suggested as electron and hole transport layers (ETL and HTL). Among the proposed ETL materials it was found that Zinc oxide (ZnO) and titanium dioxide (TiO_2) are the most adequate materials. For the HTL materials, among the proposed materials Copper (I) thiocyanate (CuSCN) forms the appropriate one. Also, the solar cell performance was improved by optimizing the absorber thickness which was found to be 1 μm. With these considerations the power conversion efficiency reached 25.02%. In addition, the detrimental effect of defects at the perovskite/TiO_2 interface on the solar cell performance is also presented.

1. Introduction

Over the years, photovoltaic technologies (PV) showed a remarkable improvement in their efficiencies. For example, solar cells based on single-crystal silicon called first generation solar cells have achieved an efficiency of up to 25% (Green et al., 2010). Solar cells based on gallium arsenide (GaAs) single crystals exhibited higher efficiencies of about 29% and 40% in single and multijunction devices, respectively (Green et al., 2010). Moreover, an alternative technology to solar cells based on silicon emerged, using polycrystalline thin films such as cadmium telluride (CdTe) and copper indium gallium selenide (CIGS) with efficiencies exceeding 20% (Green et al., 2010).

The different area of solar cell developments led to a new generation of PV technology characterized by low manufacturing cost. The interest on organic nano and meso-structured solar cells such as dye-sensitized solar cells is due to low cost active layer materials and substrates (Gratzel, 2003). Nevertheless, due to worry about long term performance these cells did not achieve mass production. Among the recent type of solar cells, perovskite solar cells (PSCs) have gained a major interest as "third generation solar cells" (Ibn-Mohammedet al., 2017). ABX_3 compounds, originated from the mineral name of calcium titanate $CaTiO_3$, belong to a perovskite-type compound. Perovskite materials have suitable material parameters for solar cells such as long electron diffusion length, high optical absorption (Haiying et al., 2018), small electron and hole effective masses, low processing temperature and strong excitonic transitions (Malyukov et al., 2016; Suneth et al., 2018). These properties make the organometallic halide perovskites based solar cells achieve comparable efficiencies to the single crystal silicon and CIGS thin films counterparts (Malyukov et al., 2016). A hybrid organic-inorganic perovskites include an organic ammonium cation A ($CH_3NH_3^+$, $NH=CHNH_3^+$, etc.), a divalent metal cation B (Pb^{2+}, Sn^{2+}, Cd^{2+}, Fe^{2+}, Co^{2+}, Cu^{2+}, etc.), and halide ions X (Cl^-, Br^-, or I^-) (Suneth et al., 2018; Yadav et al., 2015). The first perovskite solar cell (PSCs) was reported by Kojima and co-workers in 2009 (Kojima et al., 2009). They used methylammonium lead iodide ($CH_3NH_3PbI_3$, '$MAPbI_3$') and methylammonium lead bromide ($CH_3NH_3PbBr_3$, '$MAPbBr_3$') as solid sensitizers in dye-sensitized solar cells (DSSCs) with liquid electrolyte. Due to dissolving of perovskite in liquid electrolyte (Farzaneh et al., 2018), these DSSCs with short lifetime (a few minutes) showed a low power conversion efficiency of 3.13% and 3.81% for $MAPbI_3$ and $MAPbBr_3$ solar cells, respectively. In 2012 an improvement of the power conversion efficiency to 10.9% was reported in (Lee et al., 2012) using a meso-superstructured organometal halide perovskites solar cell. During 2013–2014, a "regular" structure was developed using penetrated perovskite materials (which is the light absorption region) into mesoporous metal oxide layer (that transports and collects electrons ETL such as titanium dioxide TiO_2), and was capped by another layer on the top (a hole transport material HTM) (Ibn-Mohammed et al., 2017; Malyukov et al., 2016).

In this work, several materials were studied for possible electron

* Corresponding author.
E-mail address: n.sengouga@univ-biskra.dz (N. Sengouga).

https://doi.org/10.1016/j.solener.2019.02.017
Received 6 December 2018; Received in revised form 29 January 2019; Accepted 9 February 2019

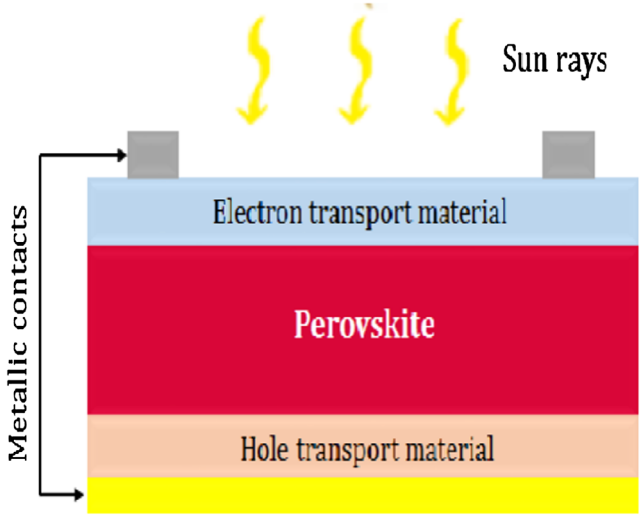

Fig. 1. The n-i-p perovskite Solar cell structure.

and hole transport layers (ETL and HTL). Organic fullerene derivative [6,6]-phenyl-C_{61}-butyric acid methyl ester (PCBM), indium gallium zinc oxide (IGZO), tin dioxide (SnO_2), titanium dioxide (TiO_2) and zinc oxide (ZnO) are tested as an ETL and compared to ITO. For the HTL materials, the proposed materials are: P3HT[poly(3-hexylthiophène-2,5-diyl), Spiro-OMeTAD (2,2′,7,7′-tetrakis-(N,N-di-p-methoxyphenyl-amine)-9,9′-spirobifluorene), CuSCN (Copper(I) thiocyanate), CuI (Copper(I) iodide) and NiO [Nickel (II) Oxide]. Furthermore, the absorber layer thickness is optimized. In addition, the detrimental effect of defects at the perovskite/TiO_2 interface on the solar cell performance will be presented.

2. Materials and methods

2.1. Device structure

The perovskite ($CH_3NH_3PbI_3$) solar cell simulated in this work is illustrated in Fig. 1. It is a one dimensional devise with n-i-p planar heterojunction. The n region is the ETL, the i-region is the perovskite layer and the p region is the HTL. When the cell is subject to light, excitons (bound state of an electron and a hole) are created mainly in the perovskite i layer. According to their diffusion length they can reach the n(p) region. At the n/i interface the exciton is dissociated and the electron moves toward the n layer while the remaining hole migrates towards the p layer. Similarly, at the i/p interface the exciton is dissociated and the hole moves to the p layer while the remaining electron migrates to the n layer. The dissociation of exitons and the migration of electrons and holes is favored by the electrical field between the n and p layers.

The input parameters of the structure and the different materials are summarized in Table 1. The primary cell has Indium tin oxide ITO as ETL and [PEDOT:PSS (Poly(3,4-ethylenedioxythiophene)-poly(styrenesulfonate))] as HTL. The absorption coefficient of the perovskite material was extracted from (Löper et al., 2015). The simulation is carried out under $AM1.5G$ solar spectrum with an incident power density of 100 mW/cm^2 at room temperature (300 K). Where, the input parameters of ITO are extracted from (Pandey and Chaujar, 2016). The perovskites and PEDOT:PSS parameters are taken from (Minemoto and Murata, 2014; Pandey and Chaujar, 2016) and (Mandadapu et al., 2017), respectively.

2.2. Numerical simulation

Numerical modeling simplifies the understanding of solar cells basics and helps identifying the major parameters which affect their performance, SCAPS-1D software (Solar Cell Capacitance Simulator One dimension) (Burgelman et al., 2018) numerically solves one dimensional equations that govern the semiconductor material under steady state conditions.

Table 1
The n-i-p perovskite Solar cell (PSC) input parameters.

Parameter	Term	ETM (ITO)	Perovskite	HTM (PEDOT:PSS)
$d(\mu m)$	*Thickness*	0.05	0.4	0.05
$E_g(eV)$	*Band gap*	3.65	1.55	2.20
χ (eV)	*Affinity*	4.8	3.9	2.9
ε_r	*Permittivity*	8.9	6.5	3.00
N_c (cm^{-3})	*Effective density of states at CB*	5.8×10^{18}	2.2×10^{18}	2.2×10^{15}
N_v (cm^{-3})	*Effective density of states at VB*	1×10^{18}	1.8×10^{19}	1.8×10^{18}
μ_n $(cm^2/V\,s)$	*Mobility of electrons*	10	2	2×10^{-2}
μ_p $(cm^2/V\,s)$	*Mobility of holes*	10	2	2×10^{-4}
N_d (cm^{-3})	*Density of n-type doping*	1×10^{20}	5.21×10^{9}	0.0
N_a (cm^{-3})	*Density of p-type doping*	0.0	5.21×10^{9}	3.17×10^{14}
N_t (cm^{-3})	*Density of defects*	1×10^{19}	2.5×10^{13}	1×10^{15}

Poisson equation which presents the relationship between electric field of a p-n junction (E) and the space charge density (ρ) is given by:

$$\frac{\partial^2\psi}{\partial^2 x} = -\frac{\partial E}{\partial x} = -\frac{\rho}{\varepsilon_s} = -\frac{q}{\varepsilon_s}[p - n + N_D^+(x) - N_A^-(x) \pm N_{def}(x)] \quad (1)$$

Where, ψ is the electrostatic potential, q is elementary charge, ε_s is the static relative permittivity of the medium, n(p) is the electron (hole) density, $N_D^+(N_A^-)$ is the density of ionized donors (acceptors) and N_{def} is the possible defect (Acceptor or donor) density (Minemoto and Murata, 2014).

The electron and hole continuity equations in steady state are given by:

$$\frac{\partial j_n}{\partial x} + G - U_n(n, p) = 0 \quad (2)$$

$$-\frac{\partial j_p}{\partial x} + G - U_p(n, p) = 0 \quad (3)$$

j_n, j_p are the electron and hole current densities; $U_{n,p}$ is the net recombination rates; G is the electron-hole generation rate.

The electron and hole current density are given by:

$$j_n = qn\mu_n E + qD_n\frac{\partial n}{\partial x} \quad (4)$$

$$j_p = qp\mu_p E - qD_p\frac{\partial p}{\partial x} \quad (5)$$

q is the elementary charge, $\mu_{n(p)}$ is electron (hole) mobility, and $D_{n(p)}$ is diffusion coefficient of electrons (holes).

SCAPS-1D software extracts the basic characteristics of the solar cell, such as the band diagram, generation and recombination rates, and cell current densities.

3. Results and discussion

The band diagram of the n-i-p PSC at equilibrium is shown in Fig. 2. An energy barrier of 0.9 eV is present between the conduction band minimum (E_c) of the ITO and the lowest unoccupied molecular orbital (LUMO) of the absorber $CH_3NH_3PbI_3$ material, and an offset about 0.35 eV between the highest occupied molecular orbitals (HOMO) of both absorber material and HTL.

The obtained current density-voltage (J-V) characteristic and quantum efficiency-wave length (QE-λ) curves are shown in Figs. 3 and 4, respectively. The electrical output parameters extracted are inserted

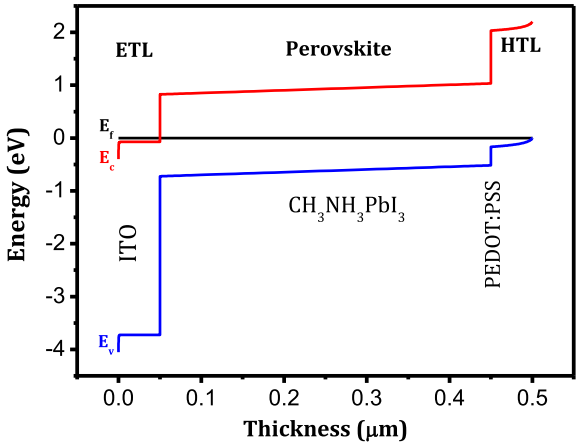

Fig. 2. The band diagram of the n-i-p PSC at equilibrium.

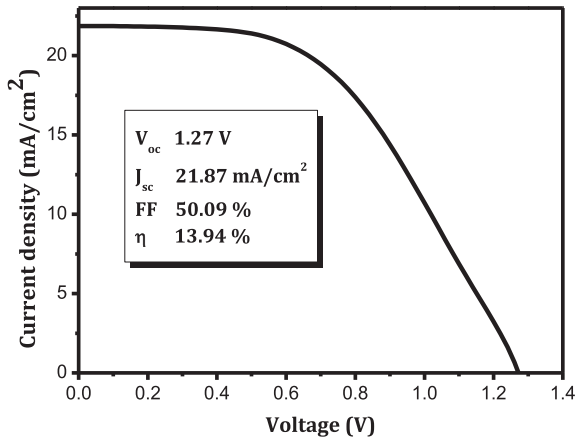

Fig. 3. J-V characteristics of the n-i-p PSC.

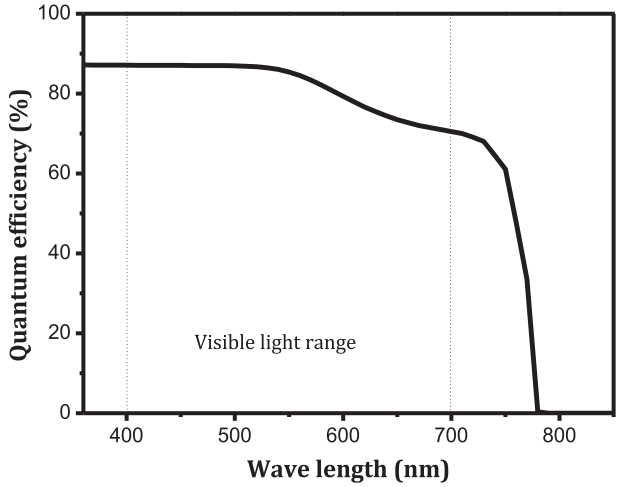

Fig. 4. The quantum efficiency of the n-i-p PSC.

in Fig. 3.The cell exhibits a slightly low fill factor (50.09%), but a good short circuit current J_{sc} = 21.87 mA/cm^2 and a remarkable open circuit voltage V_{oc} = 1.27 V (compared to the band gap energy 1.55 eV of the absorber layer). These extracted parameters gave a power conversion efficiency of 13.94%.

Quite generally, the term $\{(E_g/q) - V_{oc}\}$ that presents the bandgap-voltage offset, is a useful measure to assess the electronic quality of the absorber layer in the solar cell (Wolf et al., 2014). The small difference between E_g/q of the absorber material and V_{oc} of the corresponding solar cell indicates a low nonradiative recombination and long diffusion lengths of charge carriers due to the low exciton bounding energy (Watthage et al., 2018). A suitable quantum efficiency of $\sim 70 - 87\%$ is obtained in the visible range and is related to the good current density J_{sc} = 21.87 mA/cm^2.

The low fill factor FF noticed in the actual n-i-p PSC with PEDOT:PSS as HTL can be related to the high series resistance R_s.The low doping density of PEDOT:PSS (10^{14} cm^{-3}) lead to an increased depletion region at HTL of the device (which is a thin layer). This phenomena produces a bulk resistance of the p type material and an interfacial contact resistance between rear contact and the p type layer.

3.1. Effect of the electron transport layer

In order to obtain better performance of the perovskite solar cell a number of materials are suggested for ETL. For ETL, a 0.05 μm of organic fullerene derivative [6,6]-phenyl-C_{61}-butyric acid methyl ester (PCBM), indium gallium zinc oxide (IGZO), tin dioxide (SnO_2), titanium dioxide (TiO_2) and zinc oxide (ZnO) are studied and compared to ITO. The input parameters of PCBM, IGZO, SnO_2, TiO_2 and ZnO are taken from Wang et al. (2015), Azri et al. (2016), Mandadapu et al. (2017), Minemoto and Murata (2014) and Pandey and Chaujar (2016), respectively. These parameters are summarized in Table 2.

The obtained J-V characteristics are shown in Fig. 5 and the extracted output parameters are summarized in Table 3. According to the obtained results, the PCBM material presents the lowest current density J_{sc} 18.47 mA/cm^2 compared to the other materials and lowest quantum efficiency (QE) (Fig. 6). This performance may be due to its low electron and holes mobilities (2×10^{-1} cm^2/Vs) which affect the charge collection. On the other hand, the PCBM exhibited the highest fill factor (FF 74.98%) and a high V_{oc} = 1.26V.These parameters lead to a power conversion efficiency of 17.39%.

Indium gallium zinc oxide (IGZO) and tin dioxide (SnO_2) showed acceptable and comparable improvement in the efficiency (19.51% and 19.88%, respectively) and a high QE. It is known that the power conversion efficiency is defined by:

$$\eta = (V_{oc} \times J_{sc} \times FF)/P_{in} \quad (6)$$

where P_{in} is the incident light power. Both IGZO and SnO_2 exhibit almost the same values of the electrical outputs (V_{oc} 1.27 V, J_{sc} 21 $mA/cm^2$and FF 71%). These comparable values led to a conversion efficiency of about 19%. The band alignment of both IGZO and SnO2 with the perovskite (MAPbI3) is presented in Fig. 7. It can be seen that is no big difference between IGZO and SnO_2 (comparable affinity, Eg of SnO_2 is a bit wider than that of IGZO). Consequently, the improvement associated with these two materials may be due to their mobility values (see Table 2).

The best efficiency however is noticed for Zinc oxide (ZnO) and titanium dioxide (TiO_2) and it seem to be the best candidates for ETL.

Table 2
Input parameters of the proposed ETL materials.

Parameters	PCBM	IGZO	SnO_2	TiO_2	ZnO
$E_g(eV)$	2	3.05	3.5	3.2	3.3
$\chi(eV)$	3.9	4.16	4	3.9	4.1
ε_r	3.9	10	9	9	9
$N_c(cm^{-3})$	2.5×10^{21}	5×10^{18}	2.2×10^{17}	1×10^{21}	4×10^{18}
$N_v(cm^{-3})$	2.5×10^{21}	5×10^{18}	2.2×10^{16}	2×10^{20}	1×10^{19}
$\mu_n(cm^2/Vs)$	0.2	15	20	20	100
$\mu_p(cm^2/Vs)$	0.2	0.1	10	10	25
$N_d(cm^{-3})$	2.93×10^{17}	1×10^{18}	1×10^{17}	1×10^{19}	1×10^{18}
$N_a(cm^{-3})$	0.0	0.0	0.0	1.0	1×10^{5}
$N_t(cm^{-3})$	1×10^{15}	1×10^{15}	1×10^{15}	1×10^{15} neutral	2×10^{17} Donor, uniform 1.7eV aboveE_v

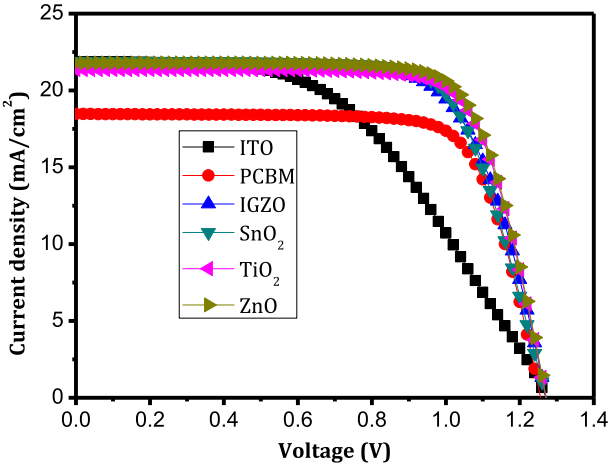

Fig. 5. Effect of the different ETL materials on J-V characteristics.

Table 3
Effect of ETLs on output parameters of the n-i-p PSC.

Parameter	ITO	PCBM	IGZO	SnO_2	TiO_2	ZnO
$V_{oc}(V)$	1.27	1.26	1.27	1.27	1.27	1.27
$J_{sc}(mA/cm^2)$	21.87	18.47	21.59	21.89	21.36	21.78
$FF(\%)$	50.09	74.98	71.08	71.43	74.66	74.53
$\eta(\%)$	13.94	17.39	19.51	19.88	20.26	20.64

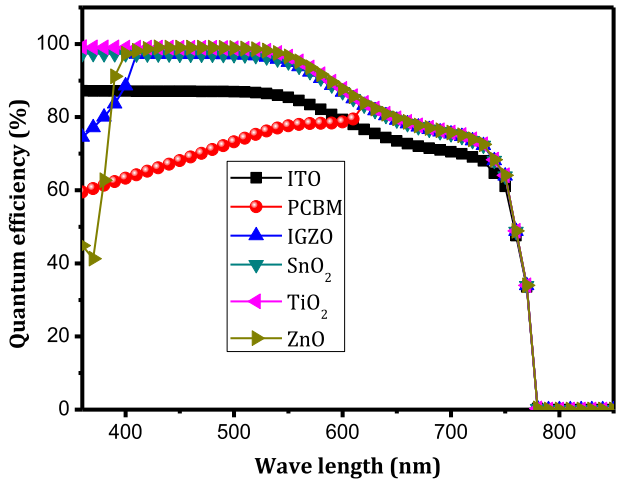

Fig. 6. Effect of the different ETL materials on quantum efficiency.

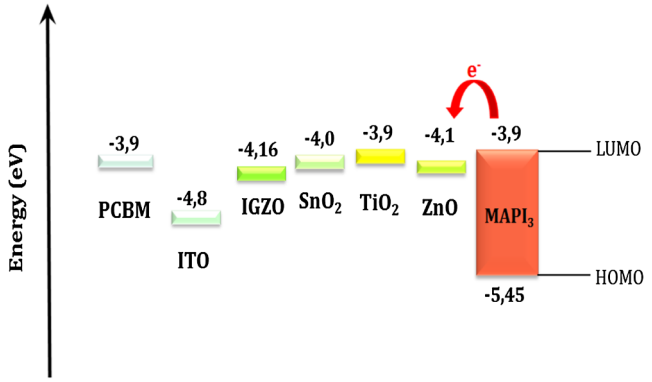

Fig. 7. Bands alignment between ETL materials and perovskite.

With an optimum compromise between the three extracted output parameters J_{sc}, V_{oc}, FF, the ZnO and TiO_2 ETL give a better conversion efficiency of about 20%. This is due to the adequate bands alignment between the conduction band of ZnO and TiO_2 and the LUMO of the perovskite as presented in Fig. 7. Also, noting that some of their input parameters seem to be similar. For example, mobility of electrons is greater in zinc oxide than in titanium dioxide (100 cm^2/Vs and 20 cm^2/Vs, respectively). But, this has been compensated by the defects density which is greater in zinc oxide than in titanium dioxide (2×10^{17} cm^{-3} and 1×10^{15} cm^{-3}, respectively).

Fig. 6 shows a decline in ZnO quantum efficiency at wave lengths $\lambda < 400nm$.This may be explained by a considerable recombination at the front surface (i.e. high defects density 10^{17} cm^{-3}) which affect the "violet and ultraviolet" portion of the spectrum, where charge carriers are not able to move into an external circuit.

3.2. Effect of the hole transport layer

In the previous section the ZnO and TiO_2 were found to be the optimum material for the ETL. Similarly in this section a number of organic and inorganic materials are investigated as HTL, first with ZnO and then with TiO_2 as ETL. The studied HTL materials are: P3HT[poly (3-hexylthiophène-2,5-diyl)], Spiro-OMeTAD (2,2′,7,7′-tetrakis-(N,N-di-p-methoxyphenyl-amine)-9,9′-spirobifluorene)], CuSCN [Copper(I) thiocyanate], CuI [Copper(I) iodide] and NiO [Nickel (II) Oxide]. The input parameters of Spiro-OMeTAD, P3HT, CuI, NiO and CuSCN are extracted from Minemoto and Murata (2014), Chen et al. (2016), Haider et al. (2018), Sajid et al. (2016) and Nanduri (2017), respectively. These parameters are presented in Table 4.

By using 0.05 μm of ZnO as ETL and changing HTL materials, the obtained J-V and quantum efficiency characteristics are presented, respectively in Figs. 8 and 9.The quantum efficiency is not affected because the optical absorption of the HTL is negligible since it is located in the back side of the device. However the J-V curves show a significant improvement of the n-i-p PSC performance. It is noticed that V_{oc} and J_{sc} were not affected. But approaching of J-V curves from the quadratic shape near J_{sc} could be explained by decreasing series resistance R_s. Also, the *HOMO* level of the $MAPbI_3$ perovskite (similar to E_v of the inorganic semiconductors) calculated from ($HOMO = \chi + E_g$) indicate that there are good bands alignment between HOMO of both of HTLs and absorber layer (Fig. 10).

The lowest power conversion efficiency is produced in the solar cell based on P3HT as HTL, because the difference between the HOMO levels of P3HT and $MAPbI_3$ reached 0.5 eV.

On the other hand CuSCN exhibited the best efficiency even if Spiro-OMeTAD exhibits the best band alignment. This is due to the holes mobility in Spiro-OMeTAD which is much smaller than holes mobility in CuSCN.

When CuSCN is used as HTL. In this case the solar cell exhibits a conversion efficiency of η 23.30% and a high fill factor of FF 83.70% as shown in Table 5.

Table 4
Input parameters of the proposed HTL materials.

Parameter	Spiro-OMeTAD	P3HT	CuI	NiO	CuSCN
$E_g(eV)$	3.00	1.85	2.98	3.6	3.4
$\chi(eV)$	2.45	3.1	2.1	1.46	1.9
ε_r	3.00	3.4	6.5	11	10
$N_c(cm^{-3})$	1×10^{19}	1×10^{22}	2.8×10^{19}	1.6×10^{19}	1.7×10^{19}
$N_v(cm^{-3})$	1×10^{19}	1×10^{22}	1×10^{19}	1.1×10^{19}	2.5×10^{21}
$\mu_n(cm^2/Vs)$	2×10^{-4}	1×10^{-4}	1.7×10^{-4}	50	1×10^{-4}
$\mu_p(cm^2/Vs)$	2×10^{-4}	1×10^{-3}	2×10^{-4}	50	1×10^{-1}
$N_d(cm^{-3})$	0.0	0.0	0.0	0.0	0.0
$N_a(cm^{-3})$	2×10^{18}	3.17×10^{13}	1×10^{18}	1.8×10^{18}	1×10^{18}
$N_t(cm^{-3})$	1×10^{15}	1×10^{14}	1×10^{15}	1×10^{14}	1×10^{14}

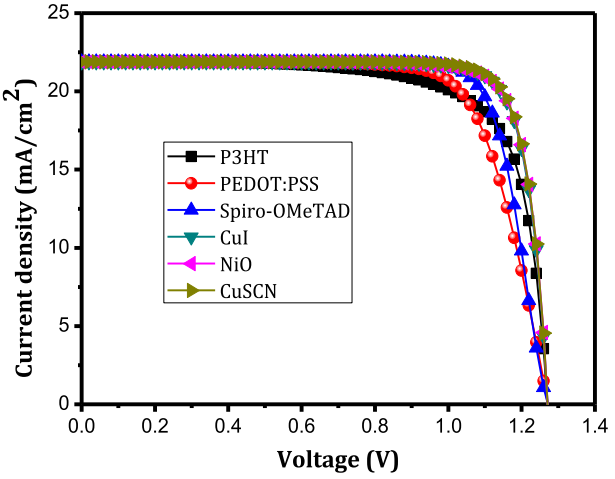

Fig. 8. Effect of different HTL materials on J-V characteristic using ZnO as ETL.

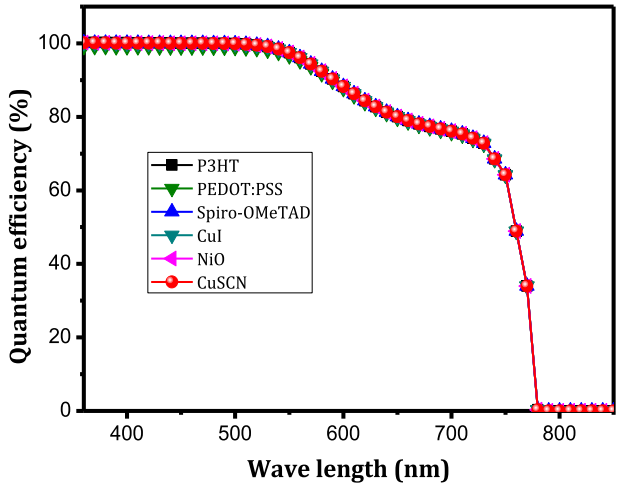

Fig. 9. Effect of the different HTL materials on quantum efficiency using ZnO as an ETL.

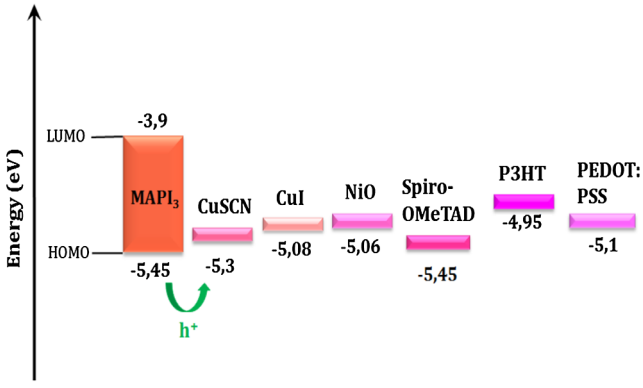

Fig. 10. Bands alignment between HTL materials and perovskite.

Table 5
Effect of the different HTL proposed materials on output parameters.

parameter	P3HT	PEDOT:PSS	Spiro-OMeTAD	CuI	NiO	CuSCN
$V_{oc}(V)$	1.27	1.27	1.27	1.27	1.27	1.27
$J_{sc}(mA/cm^2)$	21.89	21.89	21.87	21.89	21.89	21.89
$FF(\%)$	74.05	74.51	79.58	83.12	83.00	83.70
$\eta(\%)$	20.61	20.74	22.13	23.14	23.10	23.30

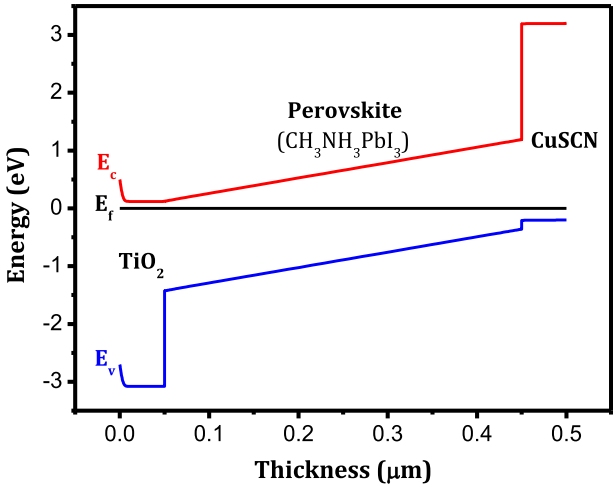

Fig. 11. The equilibrium band energy of the n-i-p PSC with TiO_2 as ETL and CuSCN as HTL.

Since in the previous section it was found that TiO_2 is a good candidate like ZnO as ETL material, we replace ZnO by TiO_2 while preserving CuSCN as HTL. The band energy diagram at equilibrium of the n-i-p PSC with the structure: FTO/TiO_2/$CH_3NH_3IPb_3$-Perovskite/CuSCN/Au, is presented in Fig. 11.

The resulting output parameters in case of TiO_2 as ETL are: $V_{oc} = 1.27\ V$, $J_{sc} = 21.89\ mA/cm^2$, $FF = 84.04\%$ and $\eta = 23.36\%$. This means an enhancement in the solar cell performance compared to the case of using ZnO as ETL of about 0.06% in power conversion efficiency and about of 0.34% in FF.

The good performance of the modeled solar cell using TiO_2 as ETL and CuSCN as HTL is associated with the good alignment of the highest occupied molecular orbital (HOMO) level of the CuSCN with the valance band of $CH_3NH_3PbI_3$. Moreover, the energy bands of ETL satisfies the following conditions: (1) its conduction band (CB) lies under the CB of the active perovskite layer to extract electrons which reach the interfaces afterward. (2) Its valence band (VB) lies much under the VB of the perovskite to reject holes. (3) ETL VB has a large difference compared to the perovskite VB in order to reject holes, because ETL has a wider band gap ($3.2\ eV$). (4) The electron mobility in ETL is sufficiently high($20\ cm^2/V.s$). Similar requirements can also be deduced for HTL.

In July 2018, the National Renewable Energy Laboratory (NREL) reported a power conversion efficiency about 23.3% (NREL, 2018) obtained lately by Institute of Chemistry–Chinese Academy of Sciences (ISCAS) for a perovskite solar cell. The conversion efficiency obtained in this work after the optimization process based on ETL and HTL materials is consequently close to what reported by (Sajid et al., 2016). It is therefore hoped that researchers workers can take the actual findings to practically realize them.

It may be possible also to even further improve the efficiency of the cell by increasing the active absorber layer (perovskite) thickness. By increasing the perovskite layer thickness to $1\ \mu m$ the conversion efficiency reaches 25.02% with a $J_{sc} = 24.70\ mA/cm^2$, due to the increase of light absorption. However, both V_{oc} and FF decrease slightly to $1.23\ V$ and 82.5%, respectively.

3.3. Effect of interfacial defects

The performance of perovskite solar cells can be altered (in most case negatively) by defect states (Fan et al., 2016). The deposition process of the perovskite solar cell can induce a formation of defects mainly located at free surface (or interface) and grain boundaries (Feng et al., 2018). These defects results from the interactions of the precursor solvents with HTL and ETL, i.e the lack of stoichiometric compositions at the surfaces of grains and the sublimation of organic molecules

Table 6
Energy position and types of interfacial defects.

Interfacial TiO_2/Perovskite defects	Energy below E_c	Charge type
Substitution defects (I_{MA})	0.75	Neutral
Oxygen Vacancy (Vo)	0.17	Donor

during the thermal annealing process could leave defects (Feng et al., 2018). Substitution defect I_{MA} (I atom occupying a MA (CH_3NH_3) site) located at − 0.75 *eV* below the conduction band is the main deep defect of perovskite films fabricated by sequential deposition method (NREL, 2018).

Another type of defects was reported by Fan Zhang and co-workers who found that oxygen vacancies at TiO_2 surface and interface could act as traps for photo-excited electrons, which affect the electrons injection and electron-hole recombination at the interface (Fan et al., 2016).

Consequently in this part, we study the effect of defects on the n-i-p PSC performance; by considering the two main types of interfacial defects: substitution defects (I_{MA}) and oxygen vacancy (Vo). The defects density is varied from 10^{10} to10^{14} cm^{-2} while theirs energy position in the band gap and charge nature are given in Table 6.

The effect of the I_{MA} and Vo defects on the J-V characteristic is shown in Figs. 12 and 13, respectively. In both cases the most sensible parameter is V_{oc} (Fig. 14) which exhibits a slight reduction caused mainly by I_{MA} defects when it reaches 10^{14} cm^{-2}. Consequently, despite that 10^{14} $cm^{-2}$is significantly high as interface density, the power conversion efficiency decreases slightly from 25.02% to 24.61% for the I_{MA} defects and to 24.95% for the Vo defects (Fig. 15).

Substitution I_{MA} defects located deeper then Vo defects have more pronounced effect on the performance of n-i-p PSC especially if the density of the defects exceeds 10^{14} cm^{-2}. These electronic states in the band gap of the semiconductor, act as Shockley-Read-Hall (SRH) recombination centers. While the oxygen vacancy (Vo) is considered as shallow defect which leads to slowing down the injection of photo excited electrons from perovskite to TiO_2 (Fan et al., 2016).

4. Conclusion

This study is an optimization of perovskite solar cell with an n-i-p configuration using SCAPS simulator. ITO/Perovskite/PEDOT:PSS structure was the primary modeled solar cell. In the first part we have examined candidate materials for ETL and HTL. Since TiO_2 and ZnO have given a high power conversion efficiency of about 23.30∼ and 23.36%, they were considered as the appropriate as ETLs while CuSCN as a suitable HTL. This was explained by the good bands alignment between the conduction band of ZnO and TiO_2 and the LUMO of the perovskite. As well as the good alignment between the HOMO level of the CuSCN and of the $CH_3NH_3PbI_3$. The band alignment is not the only parameter that affects the better efficiency of the cell, but also the mobility which plays a crucial role between materials that have almost similar band alignment proprieties.

As additional optimization the thickness of the perovskite layer was increased to 1 μm and the power conversion efficiency reached ∼25.02%.

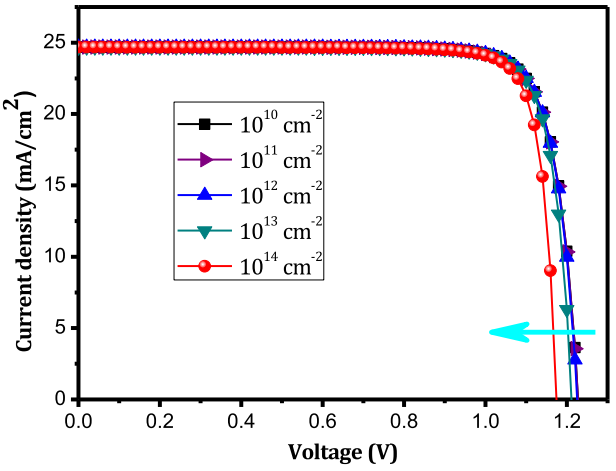

Fig. 12. Effect of I_{MA} defects on J-V characteristic.

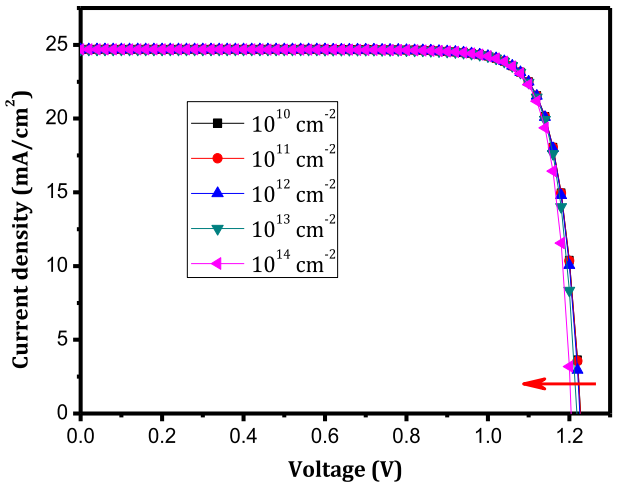

Fig. 13. Effect of Vo defects on J-V characteristic.

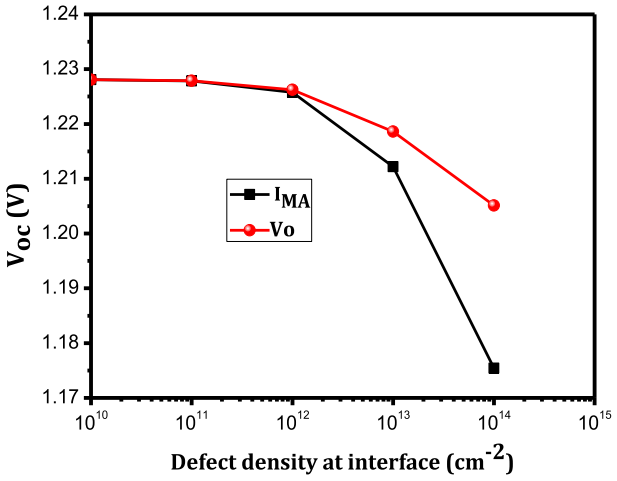

Fig. 14. Effect of I_{MA} and Vo on open circuit voltage (V_{oc}).

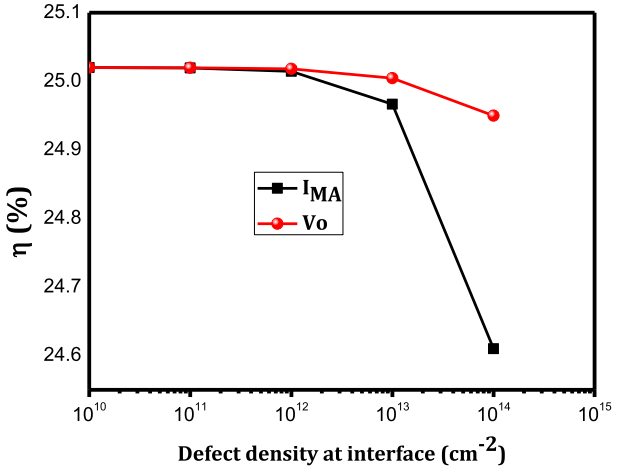

Fig. 15. Effect of I_{MA} and Vo on power conversion efficiency (η).

Finally the defect effect cannot be neglected since according the actual fabrication techniques, interfacial defects are created mainly as substitution I_{MA} and oxygen vacancy Vo. According this study their effect can becomes important mainly on V_{oc} if the interface density greatly exceeds 10^{14} cm^{-2}. These findings can be of great interest to the PSC designers.

References

Azri, F., Labed, M., Meftah, A.F., Sengouga, N., Meftah, A.M., 2016. Optical characterization of a-IGZO thin film for simulation of a-IGZO(n)/μ-Si(p) heterojunction solar cell. Opt. Quant. Electron. 48, 391.

Burgelman, M., Decock, K., Niemegeers, A., Verschraegen, J., and Degrave, S., 2018. SCAPS manual, Version: 23 January 2018.

Chen, A., Zhu, K., Shao, Q., 2016. Understanding effects of TCO work function on the performance of organic solar cells by numerical simulation. Semicond. Sci. Technol. 31, 065025 (6pp).

Fan, Z., Wei, M., Haizhong, G., Yicheng, Z., Xinyan, S., Kuijuan, J., He, T., Qing, Z., Dapeng, Y., Xinghua, L., Gang, L., Sheng, M., 2016. Interfacial oxygen vacancies as a potential cause of hysteresis in perovskite solar cells. Acs. Chemmater 5b04019.

Farzaneh, A.R., Najmeh, A., Vahid, A., Aldo, D.C., Karim, O.A., Ali, S.T., Farzaneh, S.G., Masoud, P., Nasibeh, M.R.F., 2018. Bulk heterojunction polymer solar cell and perovskite solar cell: concepts, materials, current status, and opto-electronic properties. Sol. Energy 173, 407–424.

Feng, W., Sai, B., Wolfgang, T., Anders, H., Feng, G., 2018. Defects engineering for high-performance perovskite solar cells. npj Flexible Electronics 2, 22.

Gratzel, M., 2003. Dye-sensitized solar cells. J. Photochem. Photobiol.C: Photochem. Rev. 4 (2), 145–153.

Green, M.A., Emery, K., Hishikawa, Y., Werta, W., 2010. Solar cells efficiency tables (version 35). Prog. Photovolt.: Res. Appl. 18, 144–150.

Haider, S.Z., Anwar, H., Wang, M., 2018. A comprehensive device modelling of perovskite solar cell with inorganic copper iodide as hole transport material. Semicond. Sci. Technol. 33, 035001 (12pp).

Haiying, Z., Guozhen, L., Changneng, Z., Liangzheng, Z., Ahmed, A., Tasawar, H., Xu, P., Songyuan, D., 2018. The influence of perovskite layer and hole transport material on the temperature stability about perovskite solar cells. Sol. Energy 159, 914–919.

Ibn-Mohammed, T., Koha, S.C.L., Reaneyc, I.M., Acquayed, A.G., Mustapha, K.B., Greenough, R., 2017. Perovskite solar cells: An integrated hybrid lifecycle assessment and review in comparison with other photovoltaic technologies. Renew. Sustain. Energy Rev. 80, 1321–1344.

Kojima, A., Teshima, K., Shirai, Y., Miyasaka, T., 2009. Organometal halide perovskites as visible-light sensitizers for photovoltaic cells. J. Am. Chem. SOC.131, 6050–6051.

Lee, M.M., Teuscher, J., Miyasaka, T., Murakami, T.N., Snaith, H.J., 2012. Efficient hybrid solar cells based on meso-superstructured organometal halide perovskites. Science 338, 643647.

Löper, P., Stuckelberger, M., Niesen, B., Werner, J., Filipic, M., Moon, S., Yum, J., Topic, M., De Wolf, S., Ballif, C., et al., 2015. Complex refractive index spectra of $CH_3NH_3PbI_3$ perovskite thin films determined by spectroscopic ellipsometry and spectrophotometry. J. Phys. Chem. Lett. 6, 66–71.

Malyukov, S.P., Sayenko, A.V., Ivanova, A.V., 2016. Numerical modeling of perovskite solar cells with a planar structure. Mater. Sci. Eng. 151, 012033.

Mandadapu, U., Vedanayakam, S.V., Thyagarajan, K., 2017. Simulation and Analysis of Lead based Perovskite Solar Cell using SCAPS-1D. Indian J. Sci. Technol. 10 (11).

Minemoto, T., Murata, M., 2014. Impact of work function of back contact of perovskite solar cells without hole transport material analyzed by device simulation. Curr. Appl. Phys. 14, 1428e1433.

Nanduri, S.N.R., 2017. Numerical Simulation and Performance Optimization of Perovskite Solar Cell. PhD thesis. University of Missouri.

NREL, 2018. Solar cell efficiency chart. Accessed September 2018. https://www.nrel.gov/pv/assets/pdfs/pv-efficiencies-07-17-2018.

Pandey, R., Chaujar, R., 2016. Numerical simulations: Toward the design of 27.6% efficient four-terminal semi-transparent perovskite/SiC passivated rear contact silicon tandem solar cell. Super latt. Microstruct. 100, 656–666. https://doi.org/10.1016/j.spmi.2016.10.033.

Sajid, A., Elseman, M., Ji, J., Dou, S., Huang, H., Cui, P., Wei, D., Li, M., 2016. Novel hole transport layer of nickel oxide composite with carbon for high-performance perovskite solar cells". Chin. Phys. B 25 (9), 097303.

Suneth, C.W., Song, Z., Phillips, A.B., Heben, M.J., 2018. Evolution of Perovskite Solar Cells. Elsevier Inc, University of Toledo, Toledo, OH, United States.

Wang, Y., Xia, Z., Liang, J., Wang, X., Liu, Y., Liu, C., Zhang, S., Zhou, H., 2015. Towards printed perovskite solar cells with cuprous oxide hole transporting layers: a theoretical design. Semicond. Sci. Technol. 30, 054004 (7 pp).

Watthage, S., Song, Z., Phillips, A.B., Heben, M.J., 2018. Evolution of Perovskite Solar Cells. Elsevier Inc, University of Toledo, Toledo, OH, United States 10.1016/B978-0-12-812915-9.00003-4.

Wolf, S.D., Holovsky, J., Moon, S.J., Löper, P., Niesen, B., edinsky, M., Haug, F.J., Yum, J.H., Ballif, C., 2014. Organometallic halide perovskites: sharp optical absorption edge and its relation to photovoltaic performance. J. Phys. Chem. Lett. 5, 1035–1039.

Yadav, P., Pandey, K., Bhatt, P., Raval, D., Tripathi, B., Chandra, K.P., Pandey, M.K., Kumar, M., 2015. Exploring the performance limiting parameters of perovskite solar cell through experimental analysis and device simulation. Sol. Energy 122, 773–782.